Investigation of Magnetic and Magneto-Optical Properties of Copper Cobalt Ferrite Nanoparticles

Mohammad Moradi[a, b], Forouzan Habibi[a, *], and Asiyeh Rafiee[a]

[a]Department of Physics, University of Shahrekord, Shahrekord, Iran
[b]Photonic Research Group, University of Shahrekord, Shahrekord, Iran

Corresponding author email: f.habibi@stu.umz.ac.ir

Regular Paper-Received: Feb. 27, 2024, Revised: Sept. 19, 2024, Accepted: Sept. 26, 2024, Available Online: Sept. 28, 2024, DOI: 10.61186/ijop.17.2.221

ABSTRACT— In this study, copper cobalt ferrite nanoparticles were synthesized by chemical formula $Co_{1-x}Cu_xFe_2O_4$ and (x=0, 0.2, 0.4, 0.6, 0.8, 1) by co-precipitation method. The X-ray diffraction pattern of the samples confirmed the single-phase spinel structure of the fabricated nanoparticles and the average size of the crystals was calculated from the entire width of the diffraction peak with the highest intensity and Scherrer relationship. Using transmission electron microscope images, the nanoparticle size was about 10 nm. The magnetic properties of copper cobalt ferrite nanoparticles were measured by AGFM and it was seen that with increasing substitution of copper Cations instead of cobalt Cations in the samples, the amount of induction decreased and the saturation magnetization first increased and then decreased. In order to investigate the Faraday effect on copper cobalt ferrite nanoparticles, the transmittance values were measured using a laboratory experiment and their graphs were plotted in terms of the applied magnetic field, all of which were in agreement with the theory. In addition, transmittance was investigated for two angular positions of the analyzer at -45° and +45° in different fields.

KEYWORDS: Magnetic nanoparticles, Ferrite, Co-precipitation, Faraday rotation.

I. INTRODUCTION

Spinel ferrites exhibit magneto -optical properties well. Among these properties is the Faraday effect. To investigate the Faraday effect, the nanoparticles can be used as suspension. In this method, the laser light passes through a polarizer with a definite axis of polarization (Fig. 1).

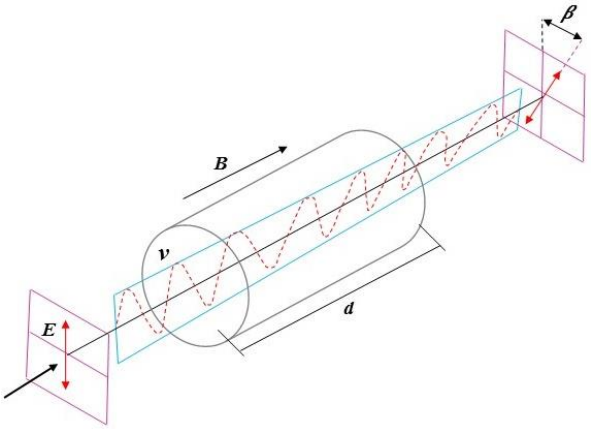

Fig. 1. The schematic scheme of Faraday effect.

The laser light then passes through a sample between the polarizer and the analyzer. Sample is under a constant magnetic field *B*. During this passage, the polarization plane of polarized laser light rotates linearly. The angle of Faraday rotation θ for a constant magnetic field is obtained from the following equation:

$$\theta = VBl \tag{1}$$

where V is the Verdt constant and depends on temperature and wavelength and l is the length of the sample. Due to the Faraday Effect, Helseth formulated a theory for magnetic fluxes. In this formula, the intensity of light transmittance after the analyzer in the presence of a magnetic field for materials with opacity is obtained from the following equation:

$$P(B) = P_0 t \cos^2(\alpha \pm \theta(B)) \tag{2}$$

where P_0 is the initial intensity of the incident light, t is the transmittance coefficient and α is

the angle between the analyzer and the polarizer. In the Faraday experiment, when the magnetic field is zero, the transmittance intensity of the transmitted light doesn't change due to the Faraday rotation, and the effect of opacity can be observed. In this case, the transmittance has minimum value. By increasing the magnetic field, the particles sample are oriented and arranged in chains in the direction of the field. Thus, The effect of opacity decreases and transmittance increases. The increase in transmittance continues to some extent and then it almost proves which the sample is saturated [1, 2]. For the synthesis of nanoparticles, various methods such as co-precipitation [3], hydrothermal [4] and sol-gel [5-7] are used. In this study, copper cobalt ferrite nano-fibers were synthesized by co-precipitation method. This method for preparing nano-ferrites has advantages such as almost uniform particle size distribution, ease of product separation, and low laboratory space required. In this method, first a solution of ferrite ions is prepared and then a suitable precipitate is added to it and then the product is separated by simple purification methods [8-11]. Spinel ferrites are widely used in electronic devices due to their magnetic permeability and high resistivity. The smallest lattice unit in the spinel structure has cubic symmetry and contains 8 molecules of $MeFe_2O_4$ in which Me represents a divalent Cation. In this structure, the large oxygen ions are very close to each other in a fcc arrangement, and the smaller ions occupy the interstitial spaces at the octahedral (B) and quadrilateral (A) positions [12]. Copper cobalt ferrite with the chemical formula $Co_{1-x}Cu_xFe_2O_4$ with cubic spinel structure has a wide range of applications in high-density data storage, MRI imaging and targeted drugs [8]. However, there has been no report on the Faraday Effect of this type of ferrite. In this study, copper cobalt ferrite nanoparticles with the chemical formula $Co_{1-x}Cu_xFe_2O_4$ (x=1, 0.8, 0.6, 0.4, 0.2, 0) were synthesized by co-precipitation method. The effect of copper substitution instead of cobalt on the structural and magnetic properties of the samples was also investigated. The main purpose of this study was to investigate the Faraday Effect for copper cobalt ferrite suspension and the effect of copper substitution instead of cobalt.

II. MATERIALS AND METHODS

Copper cobalt ferrite nanoparticles ($Co_{1-x}Cu_xFe_2O_4$, $0\leq x\leq 1$) were prepared by co-precipitation method. The chemicals used were cobalt chloride ($CoCl_{2.6}\,H_2O$), copper chloride ($CuCl_2$), iron chloride ($FeCl_3 6H_2O$) and sodium (NaOH). All materials used were made by the German company Merck and had a purity of more than 98%. First, solutions of these materials with a molar ratio of 7: 2: 1: 1 were prepared for cobalt chloride, copper chloride, iron chloride and soda with deionized distilled water, respectively. Then, according to the volumetric values according to Table 1, copper chloride, cobalt chloride and iron chloride were mixed and heated.

Table 1. Volumes of samples

Test sample	$FeCl_3 6H_2O$ (cc)	$CoCl_2 6H_2O$ (cc)	$CuCl_2$ (cc)	NaOH (cc)
$CoFe_2O_4$	20	20	0	260
$Co_{0.8}Cu_{0.2}Fe_2O_4$	20	16	4	260
$Co_{0.6}Cu_{0.4}Fe_2O_4$	20	12	8	260
$Co_{0.4}Cu_{0.6}Fe_2O_4$	20	8	12	260
$Co_{0.2}Cu_{0.8}Fe_2O_4$	20	4	16	260
$CuFe_2O_4$	20	0	20	260

This mixture of solutions was kept at a constant temperature of 90°C. The soda solution was heated separately to a constant temperature of 90°C. The metal chloride mixture was immediately added to the soda solution at 90°C, immediately a dark deposit form. At this temperature the mixture was stirred for one hour. The precipitate was then washed several times with distilled water and dispersed in distilled water at room temperature by ultrasonic device to prepare a sample suspension. According to the volumetric values of materials according to Table 1, a quantity of product is produced which can be adjusted to the concentration of samples in S_1=0.12 g/lit and S_2=0.08 g/lit. The samples were then placed in the Faraday apparatus according to Fig. 1 and the transmittance after the analyzer was measured for different angles α and θ using this arrangement. Trajectivity curves were plotted and investigated based on Helseth theory. X-ray

powder diffraction test of the samples was prepared using a PANalytical X'PertPro X-ray machine made in the Netherlands with Cu Kα radiation with a wavelength of λ=1.5406 μm. The distance between the plates, *d*, was calculated from the Bragg relation by means of diffraction peaks at an angle θ [3]:

$$n\lambda = 2d\sin\theta \quad n=1, 2, 3 \tag{3}$$

The network constant, *a*, was calculated from the peak (311) with the highest intensity from Eq. (4):

$$\frac{1}{d} = \frac{\sqrt{h^2+k^2+l^2}}{a} \tag{4}$$

where *h*, *k*, and *l* are Miller indices. The mean size of crystals *D* was calculated from the Scherrer equation:

$$\beta\cos\theta = \frac{0.9\lambda}{D} \tag{5}$$

where β is the whole width at half the maximum intensity in radians. The M-H diagram of the samples was measured by AGFM device made by Kavir Kashan Precision Magnet Company in Malekashtar University of Technology. TEM images were prepared by Zeiss EM900.

III. Results and Discussion

A. *X-ray Diffraction Pattern*

The results of the X-ray diffraction pattern of the samples are shown in Fig. 2. Analysis of X-ray diffraction pattern results of samples of copper cobalt ferrite nanoparticles using X'Pert software shows that the samples, except for the sample x=1, are single-phase and their crystal structure is cubic spinel. The peaks observed in the diffraction pattern are consistent with the reference cards 0864-003-00 and 0427-077-01.

This is shown in Fig. 3. For example, copper ferrite (x=1) has a peak that is marked with an asterisk (*) in Fig. 2. This peak corresponds to plate (111) of copper oxide with reference card 0076-080-01, which has a small probability of formation during the reaction.

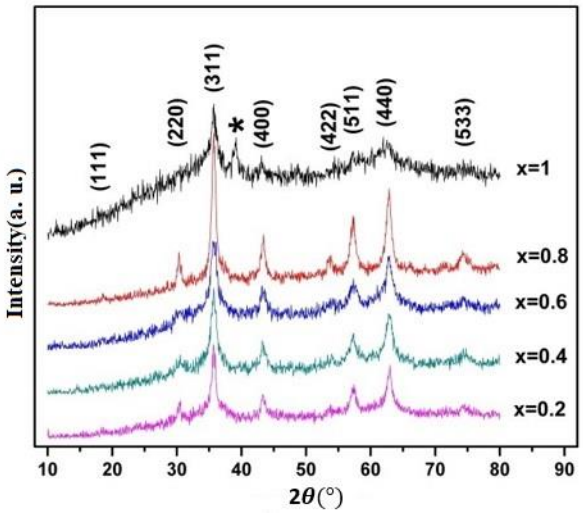

Fig. 2. X-ray diffraction pattern of copper cobalt ferrite samples. For example, there is (x=1) a peak corresponding to the plate (111) of copper oxide according to the reference card 01-080-0076, which is marked with an asterisk (*).

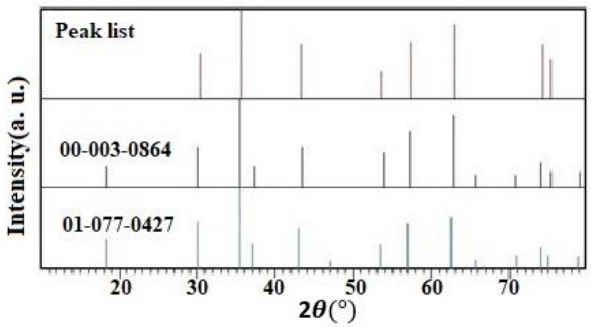

Fig. 3. Match the results of X-ray diffraction pattern and reference cards.

The results of the calculations for plate spacing, lattice constant, and mean crystal size from Eqs. 3, 4, and 5 are listed in Table 2. According to the ionic radius of copper Cation (0.87) and the ionic radius of cobalt Cation (0.74), it is observed that with the increase of copper Cation compared to cobalt Cation, the peaks move to smaller angles. The reason for this is that the size of the copper Cation is 0.13 larger than the size of the cobalt Cation and with the substitution of copper instead of cobalt, the lattice constant increases slightly and with increasing lattice constant, *a*, the distance between the plates, *d*, increases. As a result of Eq. 3, as the distance between the plates increases and the wavelength is constant, λ, the peaks must move to smaller angles.

Table 2. The results of X-ray diffraction pattern

Samples	*d* (Å)	*a* (Å)	*D* (nm)

$Co_{0.8}Cu_{0.2}Fe_2O_4$	2.514	8.322	19
$Co_{0.6}Cu_{0.4}Fe_2O_4$	1.474	8.328	10
$Co_{0.4}Cu_{0.6}Fe_2O_4$	2.511	8.312	9
$Co_{0.2}Cu_{0.8}Fe_2O_4$	2.516	8.330	16
$CuFe_2O_4$	2.513	8.319	11

B. *Morphology of Transmission Electron Microscope Images*

Figure 4 shows the transmission electron microscope (TEM) images for the $Co_{0.4}Cu_{0.6}Fe_2O_4$ sample at different magnifications. As can be seen from the pictures, the average particle size is about 10 nm. These images show that the prepared copper cobalt ferrite nanoparticles are spherical and have a uniform distribution. Given the average particle size and average crystal size for this particular sample, it is clear that most nanoparticles in this sample can be single crystals.

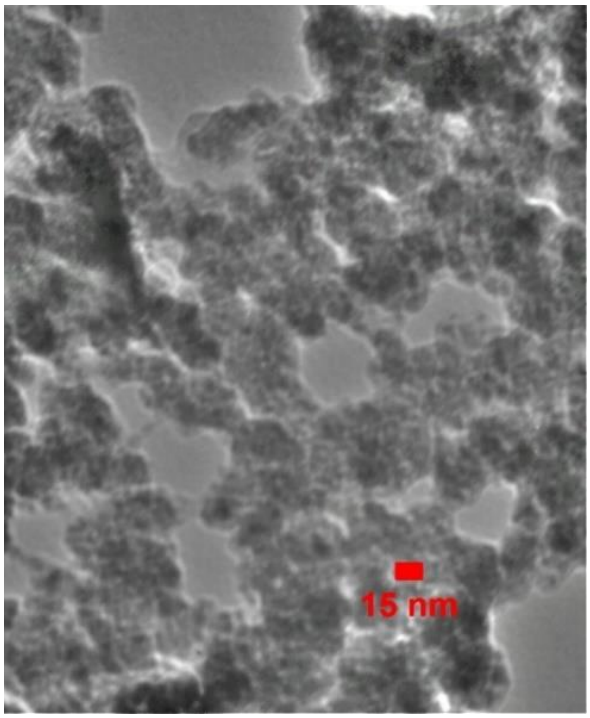

Fig. 4. The TEM images of $Co_{0.4}Cu_{0.6}Fe_2O_4$ sample.

C. *Magnetometric Result of Samples*

Figure 5 shows the M-H diagrams of the room temperature samples obtained with the AGFM. As can be seen, the samples did not reach the magnetic saturation at the maximum applied field of kOe9, which may have been formed due to the size of the nanoparticles.

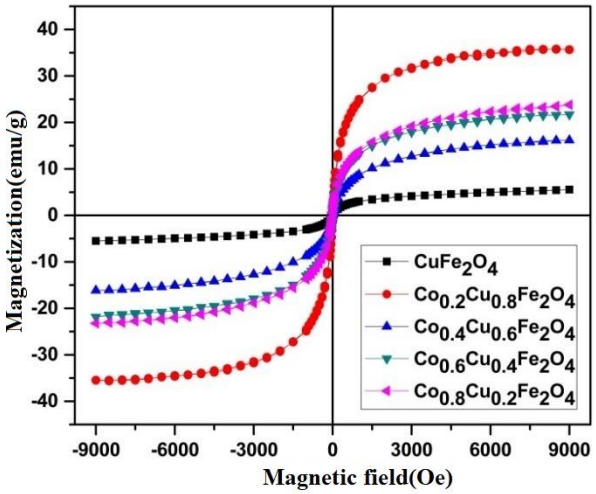

Fig. 5. The diagram of M-H samples.

The saturation magnetization of the samples was calculated from the M diagram in terms of 1/H and the extrapolation of the diagram was calculated for infinite field values. The values of saturation magnetization, residual magnetization and forcing of the samples are listed in Table 3.

Table 3. Results of magnetic property of samples

Samples	M_s (emu/g)	Mr (emu/g)	Hc (Oe)
$Co_{0.8}Cu_{0.2}Fe_2O_4$	21.8	1.4	25
$Co_{0.6}Cu_{0.4}Fe_2O_4$	23.6	0.5	9
$Co_{0.4}Cu_{0.6}Fe_2O_4$	16.2	0.2	5
$Co_{0.2}Cu_{0.8}Fe_2O_4$	35.7	1.2	10
$CuFe_2O_4$	5.9	0.1	6

Figure 6 shows a graph of saturation magnetization changes with increasing substitution of copper Cations instead of cobalt Cations. It is observed that by substituting copper ions instead of cobalt ions, the saturation magnetism first increases slightly and then have an almost decreasing trend, which loses its order with an increase in x=0.8. This increase may be due to the fact that the average crystal size of this sample is larger than samples 1, 0.6, x = 0.4, and also with the replacement of copper ions instead of cobalt ions, there is fewer cobalt ions in position B. And it is estimated that most copper ions are in the A position. As a result, iron ions can move from position A to position B, and the magnetization of the Cations at position B will be superior to that of the Cations at position A, and the total magnetization will increase. Also, the magnetization of nanoparticles due to the formation of a dead

layer on their surface according to Eq. 6 depends on their size [12-15].

$$M = M_0\left(1-\frac{t}{D'}\right)^3 \quad (6)$$

where M is the nanoparticle magnetization, M_0 is the material magnetization in the mass state, t is the thickness of the dead layer and D' is the nanoparticle size. The particle size of this sample is larger than other samples. As a result, the surface-to-volume ratio decreases and the ratio of the number of magnetic dipole moments on the surface to the volume that make up the dead layer decreases. Therefore, its magnetism can increase.

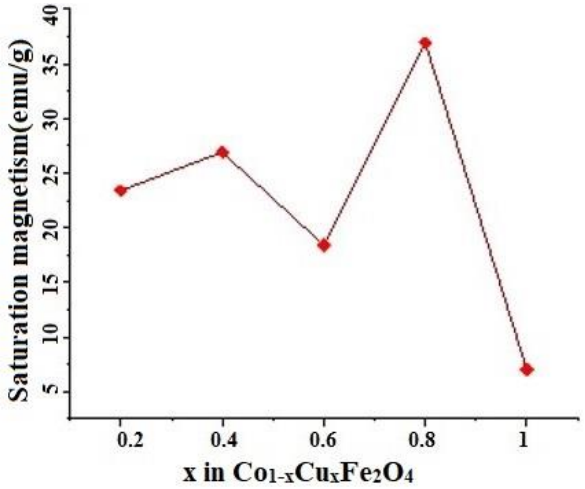

Fig. 6. Changes in saturation magnetization with increasing substitution of copper Cations instead of cobalt Cations.

Figure 7 shows a diagram of the forced changes of samples with increasing substitution of copper Cations instead of cobalt Cations. This graph shows the approximate trend of decreasing coercion in terms of increasing copper ion substitution.

We know that copper ions have a weaker magnetic interaction than cobalt ions [8], so by substituting this ion for cobalt ions, it changes the direction of magnetic dipole moments in smaller fields. For example, at x=0.8, a small increase in coercion is observed, which could confirm that the average crystal size of this sample is larger and that the distribution of copper and iron ions at positions A and B is such that iron ions at position B is in position A due to the presence of copper ions and has a stronger magnetic interaction with positions B-B.

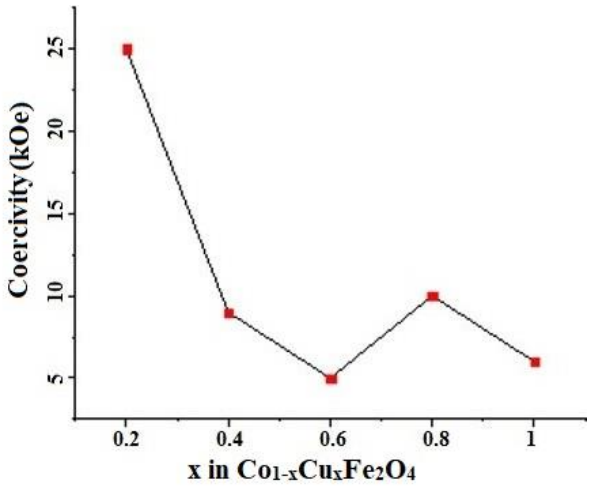

Fig. 7. Coercion changes with increasing substitution of copper Cations instead of cobalt Cations.

D. *Measurement of magneto-optical properties*

If all the components of a magnetic circuit are constant, the flux density of the magnetic field, B, will have a direct and linear ratio with the electric current passing through the circuit [16]. Transmittance after the analyzer was measured at the angles α=0˚ and α=45˚ for the samples using the Faraday Experiment which had upward trends [16]. Moreover, the results show that the transmittance changes with increasing field at angle α=90˚ also increases and confirms the theory of Helseth (Figs. 8(a) and 8(b)).

Also, by comparing parts (a) and (b) in Fig. 8, it can be seen that saturation with increasing copper concentration occurs in higher fields. This may be due to the fact that with increasing copper concentration, the effect of geometric shadow increases and the transgenicity of the sample decreases, thus reducing the response of nanoparticles to the external field. For better response, larger fields are needed. Be in the form of chains in the direction of the field. Helles theory was tested and compared for the same samples at different concentrations of S_1 and S_2. Figures 9(a), 9(b), and 9(c) show the combination diagrams of these results from different angles. The results, while confirming the associs1ation between increased transmittance and an increase in magnetic field,

show that transsaturation increases with decreasing concentration and that, as expected, thinner samples become saturated sooner.

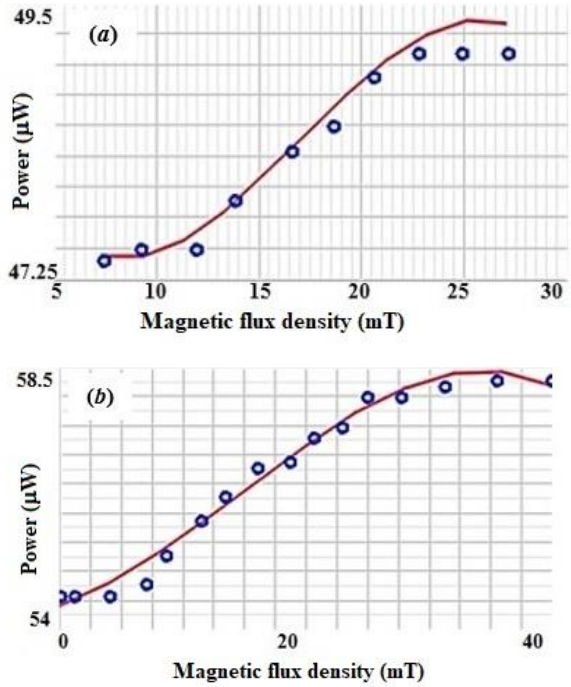

Fig. 8. The transmittance for the samples; a) $CoFe_2O_4$ and b) $Co_{0.2}Cu_{0.8}Fe_2O_4$ at concentration S_1 and α=90˚

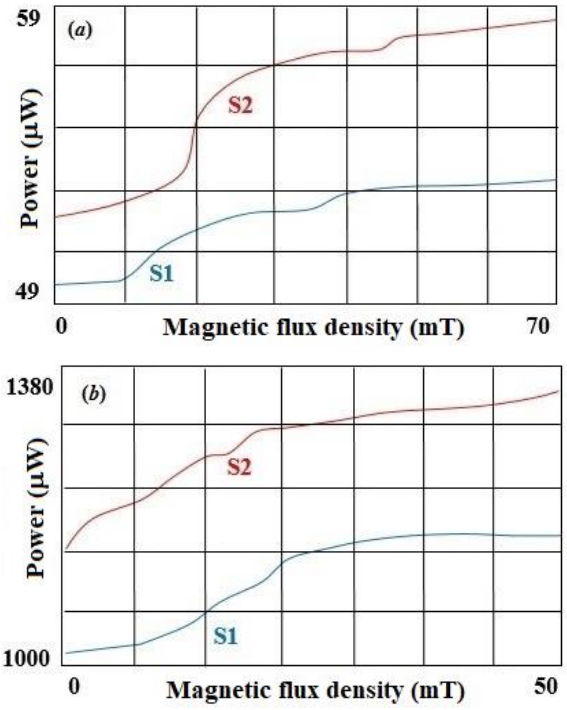

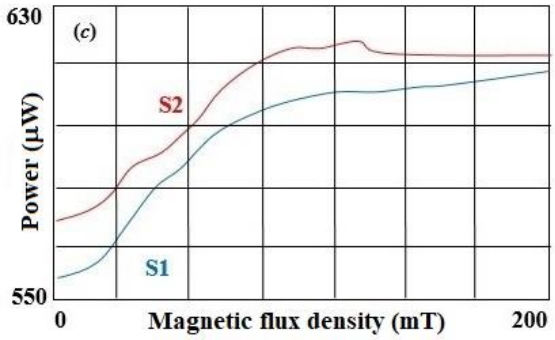

Fig. 9. The transmittance for the samples $Co_{0.8}Cu_{0.2}Fe_2O_4$ at concentration S_1 and S_2 for a) α=۰˚, b) α=۹۰˚, c) α=45˚.

E. *Calculation of Verdt constant*

Using Eq. 1, the Verdt constant can be obtained. The results for different copper substitutions are given in Table 4. As can be seen from Table 4, the input constant for all samples is constant within the test error range and no noticeable changes were observed.

Table 4. Verdt constant (rad/mT.cm) ×10^{-3}

x	1	0.8	0.6	0.4	0.2	0
Verdt	4	4	4	4	4	4

IV. CONCLUSION

The results show that the transmittance after the analyzer agrees with Helseth's theory and with increasing the magnetic field the transmittance increases to a certain value. But as the magnetic field increases further, the transmittance does not increase. This indicates the saturation of the substance. In the trajectory diagrams after the analyzer at the angles α=45˚ and α=-45˚, the difference in the saturation limit is clearly seen, which is in complete agreement with Helseth's theory. It is also observed from the results that with decreasing the concentration of the samples, the magnetic saturation decreases. In this study, it was found that according to Faraday, based on Helseth theory, magnetic saturation and transmittance are directly related, that is, with increasing magnetic field and saturation of transmittance also increases.

REFERENCES

[1] G. Fowles, *Introduction to Modern Optics*, Holt Rinehart and Win, 2nd Ed., pp. 1-336, 1968.

[2] E. Hecht, *Optics, Pearson Global*, 5th Ed., pp. 1-714, 2017.

[3] S.S. Nair, F Xavier, P.A. Joy, S.D. Kulkarni, and M.R. Anantharaman, "Enhanced shape anisotropy and magneto-optical birefringence by high energy ball milling in $Ni_xFe_{1-x}Fe_2O_4$ ferrofluids," J. Magn. Magn. Mater, Vol. 320, pp. 815–820, 2008.

[4] N. Sanpo, J. Wang, and C.C. Berndt, "Sol-Gel Synthesized Copper-Substituted Cobalt Ferrite Nanoparticles for Biomedical Applications," J. Nano. Res, Vol. 22, pp. 95-106, 2013.

[5] A. Hajdú, E. Illés, E. Tombácz, and I. Borbáth, "Surface charging, polyanionic coating and colloid stability of magnetite nanoparticles," Colloids Surf. A: Physicochem. Eng. Asp., Vol. 347, pp. 104–108, 2009.

[6] J.X. Kesse, A. Adam, S.B. Colin, D. Mertz, E. Larquet, T. Gacoin, I. Maurin, C. Vichery, and J.M. Nedelec, "Elaboration of Superparamagnetic and Bioactive Multicore–Shell Nanoparticles (γ-Fe_2O_3@SiO_2-CaO): A Promising Material for Bone Cancer Treatment," ACS Appl. Mater. Interfaces, Vol. 12, pp. 47820(1-23), 2020.

[7] S. Moghaddasi, A. Fotovat, F. Karimzadeh, H. R. Khazaei, R. Khorassani, and A. Lakzian, "Effects of coated and non-coated ZnO nano particles on cucumber seedlings grown in gel chamber," Arch. Agron. Soil Sci, Vol. 63, pp. 1108(1-26), 2017.

[8] M. Moradi, S. Manouchehri, and S. Kiani, "Magneto-optical properties of Co-Zn ferrite thin films," J. Opt. Technol., Vol. 83, pp. 419-421, 2016.

[9] S. Gautam, S. Muthurani, M. Balaji, P. Thakur, D. Pathinettam Padiyan, K. H. Chae, S.S. Kim, and K. Asokan, "Electronic Structure Studies of Nanoferrite $Cu_xCo_{1-x}Fe_2O_4$ by X-ray Absorption Spectroscopy," J. Nanosci. Nanotechnol., Vol. 11, pp. 386–390, 2011.

[10] A. Samavati and A.F. Ismail, "Antibacterial properties of copper-substituted cobalt ferrite nanoparticles synthesized by co-precipitation method," Particuology, Vol. 30, pp. 158-163, 2017.

[11] S. Chen, B. Mulgrew, and P.M. Grant, "A clustering technique for digital communications channel equalization using radial basis function networks," IEEE T. Neural Netw., Vol. 4, pp. 570–578, 1993.

[12] P. Kumar, P. Mahajan, R. Kaur, and S. Gautam, "Nanotechnology and its challenges in the food sector: a review," Mater. Today Chem., Vol. 17, pp. 100332(1-17), 2020.

[13] B.D. Cullity and C.D. Graham, *Introduction to Magnetic Materials*, John Wiley and Sons, 2nd Ed. pp. 1-568, 2009.

[14] H.M. El-Sayed, I.A. Alib, A. Azzam, and A.A. Sattar, "Influence of the magnetic dead layer thickness of Mg-Zn ferrites nanoparticle on their magnetic properties," J. Magn. Magn. Mater., Vol. 424, pp. 226-232, 2017.

[15] R. Desai, V. Davariy A.K. Parekh, and R.V. Upadhyay, "Structural and magnetic properties of size-controlled $Mn_{0.5}Zn_{0.5}Fe_2O_4$ nanoparticles and magnetic fluids," J. Phys., Vol. 73, pp. 765-780, 2009.

[16] M. Moradi, A. Rafiei, and S. Manoochehri, "Magneto optical properties of copper-cobalt ferrite nanoparticles under the influence of a low magnetic field," ICOP & ICPET, Vol. 23 pp. 645-648, 2017.

Mohammad Moradi received his B.Sc. in physics from Isfahan University, Isfahan, Iran, in 1989; M.Sc. in Atomic Physics from Polytechnic Tehran University, Iran, in 1992, and PhD in Atomic Physics, Optics and Laser from Moscow State University, Russia, in 2005. He is currently engaged as an assistant professor of physics in Department of Physics, Shahrekord University.

Forouzan. Habibi (b. 1991) received her M.Sc. degree in atomic and molecular physics from Sharekord University, Sharekord, Iran, in 2017, and her Ph.D. degree from Mazandaran University, Mazandaran, Iran, in 2023. Her research interests include: optics, photonics, magneto optics, and nonlinear optics. She works as a researcher at Shahrekord University and she is also a research fellow at Brescia University, Italy.

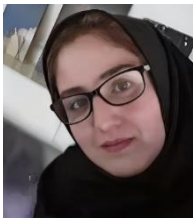

Asieh Rafiee (b. 1989) received her M.Sc. degree in atomic and molecular physics from Sharekord University, Sharekord, Iran. in 2017. Her research interests include: optics, magneto optics, and nonlinear optics.